One-body energy dissipation in fusion reactions from mean-field theory

Kouhei Washiyama,[1] Denis Lacroix,[1] and Sakir Ayik[2]
[1]*GANIL, Bd Henri Becquerel, BP 55027, F-14076 Caen Cedex 5, France*
[2]*Physics Department, Tennessee Technological University, Cookeville, Tennessee 38505, USA*
(Received 25 November 2008; published 18 February 2009)

Information on dissipation in the entrance channel of heavy-ion collisions is extracted by the macroscopic reduction procedure of time-dependent Hartree-Fock theory. The method gives access to a fully microscopic description of the friction coefficient associated with the transfer of energy from the relative motion toward intrinsic degrees of freedom. The reduced friction coefficient exhibits a universal behavior, i.e., almost independent of systems investigated, whose order of magnitude is comparable with the calculations based on linear response theory. Similarly to nucleus-nucleus potential, especially close to the Coulomb barrier, there are sizable dynamical effects on the magnitude and form factor of the friction coefficient.

DOI: 10.1103/PhysRevC.79.024609 PACS number(s): 25.70.Jj, 21.60.Jz

I. INTRODUCTION

The discovery of deep inelastic collisions in the 1970s, in which a large amount of kinetic energy and angular momentum is dissipated from the relative motion to intrinsic excitations of colliding nuclei, brought us the concept of friction in nuclear physics [1]. After this discovery, Gross and Kalinowski developed the surface friction model (SFM) [2] that takes into account this dissipative effect by introducing friction forces in a Newtonian equation. More generally, dissipative aspects in self-bound systems such as nuclei have important roles in many physical phenomena such as fission, fusion reactions, and giant resonances.

In most actual models that include dissipation and that are used to describe nuclear reactions at energies around the Coulomb barrier, the dissipation mechanism is assumed to be a one-body type, where energy dissipation is caused by collision of nucleons with the mean-field wall and by nucleon exchange between the two partners of the reaction. These effects are known as the wall-and-window formula [3,4] and are essentially based on classical consideration. The orders of magnitude of parameters related to dissipation are generally adjusted to reproduce experiments. However, large uncertainty on those parameters exists [5]. Therefore, the description of energy dissipation from quantum microscopic models is highly desirable.

It is known that the time-dependent Hartree-Fock (TDHF) model [6,7] includes a one-body dissipation mechanism from the microscopic point of view, because of the treatment of the self-consistent mean field. It is worth mentioning that the so-called fusion window problem due to underestimation of energy dissipation in old TDHF calculations has been solved by including spin-orbit interactions and time-odd terms in the energy density functional [8–10] as well as by breaking symmetries. Now three-dimensional TDHF calculations including full Skyrme effective interaction, which are used in recent static Hartree-Fock calculations, are expected to provide a better description of dissipative aspects [10–13]. Up to now, there have only been a few studies dedicated to extracting friction coefficients associated with one-body energy dissipation from the microscopic mean-field approach [6,14]. The aim of this article is to investigate the energy dissipation mechanism in detail from a microscopic point of view by using state of the art TDHF theory.

In Refs. [15] and [16], a method of extracting the nucleus-nucleus potential and friction coefficient from TDHF has been proposed. This method, called Dissipative Dynamics TDHF (DD-TDHF), assumes that mean-field evolution can be properly reduced to one-dimensional dissipative dynamics for relative distance R between nuclei. In Ref. [16], the nucleus-nucleus potential for symmetric and asymmetric reactions has been systematically extracted from the DD-TDHF. In this work, we focus on the friction coefficient, which also comes as an output of the macroscopic reduction procedure.

The article is organized as follows. In Sec. II, we briefly explain the DD-TDHF method. In Sec. III, we illustrate the main properties of the extracted friction coefficients for different systems. In Sec. IV, we discuss a method to estimate the intrinsic excitation of colliding nuclei and compare the result to the dissipated energy. A summary is given in Sec. V.

II. DESCRIPTION OF THE DD-TDHF METHOD

The DD-TDHF method, originally proposed in Refs. [6] and [15], relies on the hypothesis that complex microscopic mean-field evolution of head-on collisions can be accurately reduced into a simple one-dimensional macroscopic evolution given by

$$\frac{dR}{dt} = \frac{P}{\mu(R)}, \tag{1}$$

$$\frac{dP}{dt} = -\frac{dV}{dR} - \frac{d}{dR}\left(\frac{P^2}{2\mu}\right) - \gamma(R)\dot{R}. \tag{2}$$

R and P denote here the relative distance and relative momentum between two nuclei, respectively, and are computed from mean-field theory according to the procedure described in Refs. [15] and [16]. In the second equation, $V(R)$ and $\gamma(R)$ denote the nucleus-nucleus potential and friction coefficient, respectively, while term $-d_R(P^2/2\mu)$ arises from possible relative distance dependence of the reduced mass $\mu(R)$. The nucleus-nucleus potential for symmetric and asymmetric

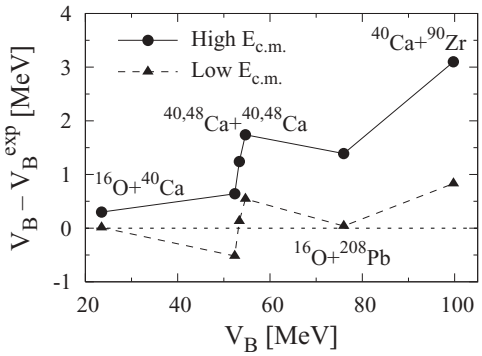

FIG. 1. Barrier height extracted from DD-TDHF minus experimental barrier height as a function of extracted barrier height for reactions indicated in the figure. V_B is deduced from high c.m. energy (solid line) and from low c.m. energy TDHF (dashed line) reactions, respectively (Values of different barrier heights can be found in Table I of Ref. [16]).

reactions deduced from the DD-TDHF method has been systematically investigated in Ref. [16]. Technical details of the method are extensively discussed in this reference and we recall here the main conclusions of the potential study: (i) We have shown in Ref. [16] that the second term in the right-hand side of Eq. (2), i.e., term involving R-derivative of reduced mass, has a minor role in the extracted nucleus-nucleus potential and can be neglected. This is also true here for relative distance larger than the barrier position, denoted by R_B. In the following, we mainly focus on $R \geqslant R_B$, where the effect of the reduced mass R dependence on friction coefficient is negligible. (ii) The DD-TDHF method gives results similar to those of the density-constrained TDHF (DC-TDHF) method at similar c.m. energy [17]. (iii) As the beam energy increases, the extracted potential tends toward the frozen density (FD) approximation, which is also expected because that density has no time to reorganize as the nuclei collide. (iv) As c.m. energy approaches the Coulomb barrier, dynamical effects induce a reduction of the barrier height, which is in agreement with the fusion threshold deduced from TDHF in Ref. [18] and is in close agreement with the experimental barrier height, see Fig. 1. In this figure, the solid line corresponds to the potential height extracted using high c.m. energy TDHF trajectories ($E_{\text{c.m.}} \gg V_B$), whereas the dashed line stands for barriers obtained when c.m. energy used in the DD-TDHF approaches the Coulomb barrier ($E_{\text{c.m.}} \sim V_B$). Dynamical reduction of the barrier height is clearly seen for all reactions. Because of this reduction, the estimated barrier height at low energy becomes much closer to barriers extracted from experiments. In summary, investigations of Ref. [16] have shown that the simple macroscopic reduction method of DD-TDHF can provide a useful tool to infer nucleus-nucleus potentials from microscopic mean-field theory. Employing the same method, we can extract information about the one-body dissipation mechanism, which is the topic of this article.

For TDHF calculations, we use the three-dimensional TDHF code developed by P. Bonche and coworkers with the SLy4d Skyrme effective force [11]. The mesh sizes in space and time are 0.8 fm and 0.45 fm/c, respectively. As TDHF initial conditions, we solve static HF equations [19,20] with the same effective force and the same mesh size as in TDHF. The initial distances between two nuclei are set between 16 and 22.4 fm. We assume that colliding nuclei follow the Rutherford trajectory before they reach the initial distance for TDHF calculations.

III. FRICTION COEFFICIENTS FROM MEAN-FIELD DYNAMICS

A. Friction coefficient at c.m. energy well above the Coulomb barrier

In addition to the nucleus-nucleus potential, one-dimensional macroscopic reduction gives also access to the friction coefficient $\gamma(R)$. We first focus on friction coefficients extracted from TDHF calculations when c.m. energy is well above the Coulomb barrier, i.e., for which extracted potentials identify with FD potentials [16]. Possible c.m. energy dependence of dissipation is discussed later.

Figure 2 presents an important result of this work. The reduced friction coefficients, defined as $\beta(R) = \gamma(R)/\mu(R)$, are extracted from a fully microscopic theory without any free parameter adjustment or adiabatic/diabatic assumption. Reduced friction coefficients are systematically shown for the mass symmetric reactions (upper panel) $^{40}\text{Ca} + {}^{40}\text{Ca}$ and $^{48}\text{Ca} + {}^{48}\text{Ca}$ and mass asymmetric reactions (lower panel) $^{16}\text{O} + {}^{40,48}\text{Ca}$, $^{16}\text{O} + {}^{208}\text{Pb}$, $^{40}\text{Ca} + {}^{48}\text{Ca}$, and $^{40}\text{Ca} + {}^{90}\text{Zr}$ as a function of relative distance. As the colliding nuclei approach each other, reduced friction coefficient monotonically increases and is almost independent of colliding system. Therefore, a universal behavior of the friction coefficient is observed in collisions at c.m. energies well above the Coulomb barrier.

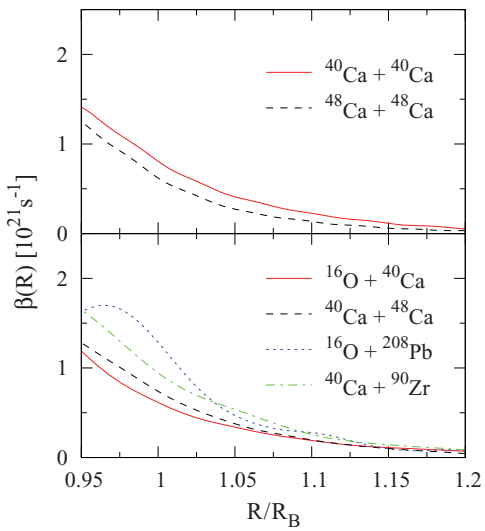

FIG. 2. (Color online) Reduced friction coefficient $\beta(R) = \gamma(R)/\mu(R)$ as a function of R divided by the Coulomb barrier radius R_B for mass symmetric (upper panel) and mass asymmetric (lower panel) reactions.

B. Energy dependence of friction coefficient

As c.m. energy approaches the Coulomb barrier, dynamical effects such as deformation and neck formation can take place. These aspects are automatically included in dynamical mean-field calculations and have been shown to systematically reduce the barrier compared to the high energy limit. Similarly to potential energy landscape, we do expect dissipation to be modified as the beam energy decreases. Figure 3 shows the extracted friction coefficient obtained using different c.m. energies between 55 and 100 MeV for the $^{40}\mathrm{Ca}+{}^{40}\mathrm{Ca}$ reaction. We note that the Coulomb barrier energy of this reaction extracted at c.m. energy $E_{\mathrm{c.m.}}=55$ MeV is about 53 MeV. Similarly to potential landscape, which tends to the FD case as the beam energy increases, we observe that the magnitude of friction coefficient does not change as the c.m. energy increases between $E_{\mathrm{c.m.}}=90$ and 100 MeV. The associated dissipation corresponds to limited situations when density has no time to reorganize in the entrance channel.

On the other hand, for $E_{\mathrm{c.m.}}=55$ and 57 MeV, which are close to the Coulomb barrier, the friction coefficient exhibits sizable energy dependence. The lower the energy is the larger the magnitude of friction. The radial dependence of the friction coefficient is very different from that at high energies. At low energies, the friction coefficient shows a peak near the Coulomb barrier and decreases to smaller values inside the Coulomb barrier, which is located around $R=R_B\approx 10$ fm.

The enhanced dissipation around the Coulomb barrier energies is partly due to early neck formation accompanied by an increase of nucleon exchange. This is illustrated in Fig. 4, where the number of nucleons transferred from one nucleus to the other is shown as a function of R for the $^{40}\mathrm{Ca}+{}^{40}\mathrm{Ca}$ reaction at the same energies as in Fig. 3. For such a symmetric reaction, the separation plane is located at $x=0$. The number of nucleons initially in the projectile (taken by convention at initial time at $x<0$) having passed through the separation plane, i.e., transferred to the target, is estimated by

$$N^{P}_{\mathrm{trans}}[R(t)]=\int d^3x\,\rho_P(\mathbf{r},t)\,\theta(x), \tag{3}$$

where ρ_P (resp. ρ_T) are defined through

$$\rho_{P/T}(\mathbf{r},t)=\sum_{i\in P/T}|\phi_i(\mathbf{r},t)|^2, \tag{4}$$

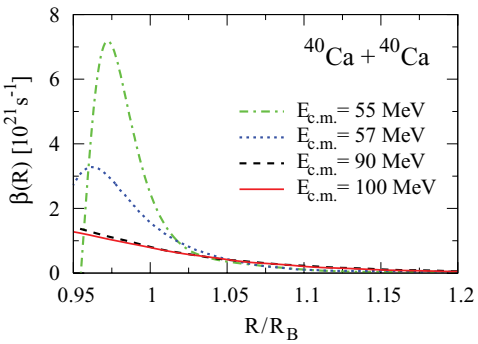

FIG. 3. (Color online) Reduced friction coefficient as a function of R/R_B for the $^{40}\mathrm{Ca}+{}^{40}\mathrm{Ca}$ reaction at different c.m. energies.

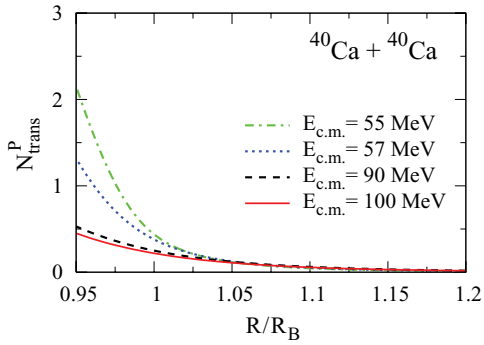

FIG. 4. (Color online) Number of nucleons transferred from projectile to target $N^{P}_{\mathrm{trans}}[R(t)]$ as a function of R for the $^{40}\mathrm{Ca}+{}^{40}\mathrm{Ca}$ reaction at c.m. energies the same as those in Fig. 3.

with $\phi_i(\mathbf{r},t)$ being the single-particle wave function initially in the projectile (resp. target) and propagated through the mean field. $\theta(x)$ is the step function equal to zero for negative x and 1 for positive x. We can equivalently define the number of nucleons transferred from target to projectile, denoted by N^{T}_{trans}. For symmetric reactions, N^{P}_{trans} is equal to N^{T}_{trans} at all times. For $R\geqslant R_B$, the enhancement of dissipation observed in Fig. 3 is strongly correlated to the increase of particle exchange. Such a strong correlation is indeed expected from the window dissipation mechanism [4], in which the magnitude of the friction coefficient is proportional to the window area, and hence the number of nucleons exchanged through the window. From the strong similarity between Figs. 3 and 4, one can conclude that the main source of dissipation at large distance ($R\geqslant R_B$) is due to nucleon exchange.

Enhancement of dissipation at low c.m. energy is systematically observed as seen in Fig. 5, where the reduced friction coefficient $\beta(R)$ is plotted as a function of relative distance. It also appears that enhancement of dissipation before the barrier

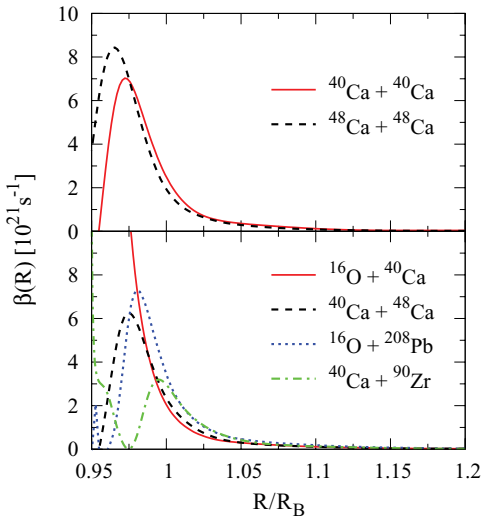

FIG. 5. (Color online) Reduced friction coefficient $\beta(R)=\gamma(R)/\mu(R)$ as a function of R divided by Coulomb barrier radius R_B for mass symmetric (upper panel) and mass asymmetric (lower panel) reactions. In each case, the c.m. energy used to extract the friction coefficient corresponds to the Coulomb barrier energy.

$R \geqslant R_B$ is nearly independent of the systems investigated. For instance near barrier $R/R_B = 1$, the magnitude of friction at high energy is about $\beta(R) \equiv 0.8 \times 10^{21}$ s^{-1}, while at near barrier energies, its magnitude is about four times larger, $\beta(R) \equiv 3 \times 10^{21}$ s^{-1}, for all systems investigated.

For all the systems investigated, calculations show that the magnitude of friction coefficient rapidly decreases for decreasing relative distances $R < R_B$. We believe that this unphysical behavior is due to simple macroscopic reduction procedure, which breaks down at low energies, when colliding nuclei begin to overlap strongly. In this case, complex dynamical effects such as the onset of nuclear deformation [16] and non-Markovian effects become important in the dissipation mechanism, which are not incorporated in the simple reduction procedure presented here.

C. Comparison with other models

There is large uncertainty between microscopic and phenomenological descriptions of nuclear dissipation [5]. Therefore it is of great interest to provide an accurate description of nuclear dissipation. The macroscopic reduction presented in this work provides a useful insight toward that goal. In this section, we compare our results with those of the macroscopic surface friction model (SFM) [2] and the microscopic calculations of Adamian *et al.* [21]. The SFM was introduced in a classical description of relative motion in deep inelastic heavy-ion collisions in Ref. [2]. The radial friction force was parametrized as $\gamma(R) = K_r(dV_N/dR)^\alpha$, where V_N is the nuclear part of the nucleus-nucleus potential and K_r and α are parameters. These parameters were fitted as $K_r = 4 \times 10^{-23}$ s/MeV and $\alpha = 2$. Microscopic calculations of Ref. [21] are based on the linear response theory of nuclear dissipation [22]. These calculations take into account time evolution of single-particle occupation factors during collision through a consistent treatment of the collective and intrinsic degrees of freedom.

In Fig. 6, high energy (solid line) and low energy (dot-dashed line) DD-TDHF results are compared both with the SFM case (solid triangles) and an example of linear response theory results obtained in Ref. [21] (solid circles). It is observed that at $R \approx R_B$ the SFM strongly overestimates the magnitude of the friction coefficient compared to the other microscopic models, while our result agrees at high c.m. energy with the microscopic calculations of Ref. [21] (solid circles).

IV. DISSIPATED ENERGY, NUCLEON EXCHANGE, AND EXCITATION ENERGY IN NUCLEI

In this section, we discuss the link between internal excitation energy of colliding nuclei and dissipated energy from the macroscopic degrees of freedom. In addition, we give further evidence for the fact that particle transfer is the main source of dissipation before two nuclei reach the Coulomb barrier.

A. Total energy dissipation

From energy conservation, we can give a simple estimate of dissipated energy $E_{\rm diss}$ in the entrance channel as

$$E_{\rm diss} = E_{\rm c.m.} - \frac{P^2}{2\mu} - V^{\rm DD}(R), \tag{5}$$

where the second term is nothing but the relative kinetic energy while $V^{\rm DD}$ denotes the potential extracted from the DD-TDHF method. Figure 7 illustrates the magnitude of different quantities as a function of relative distance for the ^{40}Ca + ^{40}Ca reaction at $E_{\rm c.m.} = 100$ MeV. According to Eq. (2), we can calculate dissipated energy from the friction coefficient γ using the Rayleigh formula

$$E_{\rm diss}(R(t)) = \int_0^t dt'\, \gamma(R(t'))\,[\dot{R}(t')]^2, \tag{6}$$

where $\dot{R}$ denotes the relative velocity deduced from mean-field evolution. We have checked that the above equation gives results identical to those of Eq. (5).

The dissipated energy provides a measure for the transfer of energy from relative motion to internal degrees of freedom

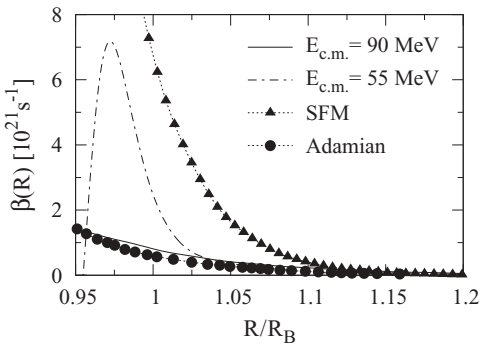

FIG. 6. Comparison between the reduced friction coefficient deduced with the DD-TDHF method for the ^{40}Ca + ^{40}Ca reaction at $E_{\rm c.m.} = 90$ MeV (solid line) and the one computed by Adamian *et al.* [21] for the ^{64}Zn + ^{196}Pt reaction at $E_{\rm lab} = 440$ MeV (solid circles). The results of SFM [2] for the ^{40}Ca + ^{40}Ca reaction are also presented by solid triangles.

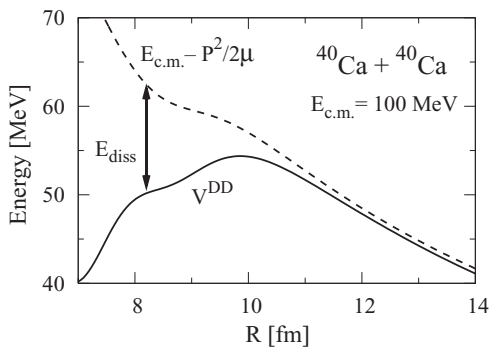

FIG. 7. Evolution of potential $V^{\rm DD}$ extracted from the DD-TDHF as a function of R (solid line) for the ^{40}Ca + ^{40}Ca reaction at $E_{\rm c.m.} = 100$ MeV. The difference between total c.m. energy and relative kinetic energy is also shown by the dashed line. The difference between the two curves is nothing but dissipated energy in the entrance channel.

during the collision. Denoting by E^* the internal excitation energy and assuming that all dissipated energy is converted into internal excitation energy, we do expect $E^* = E_{\rm diss}$. In the following, we apply a method to estimate directly the internal excitation energy of the projectile and target during the early stages of collision and show that a good agreement is obtained with the amount of dissipated energy.

B. Estimate of internal excitation energy

1. Single nucleus case

For a single isolated nucleus, in the mean-field approach, the excitation energy can be estimated using

$$E^* = \mathcal{E}^{\rm ex}_{\rm MF} - \mathcal{E}^{0}_{\rm MF}, \tag{7}$$

where $\mathcal{E}^{0}_{\rm MF}$ and $\mathcal{E}^{\rm ex}_{\rm MF}$ denote ground state and excited state mean-field energy, respectively. For small excitations, we can approximately calculate the excitation energy according to

$$E^* \simeq \sum_i \left(\varepsilon^0_i - \varepsilon^\tau_F\right) \times \left(n_i - n^0_i\right). \tag{8}$$

In this expression, ε^0_i denotes single-particle energies, ε^τ_F, with $\tau = n$, p stands for the neutron or proton Fermi energy, while n_i and n^0_i are the occupation factors in the excited and the ground state, respectively.

2. Dinucleus case

In the case of two colliding nuclei, we are mainly interested in the entrance channel ($R \geqslant R_B$) where the two nuclei slightly overlap. In this dinuclear configuration, we define the collective variables by drawing the separation plane as illustrated in Fig. 8. In the entrance channel, colliding nuclei are weakly excited. To calculate the excitation energy of each partner using the lowest order perturbation expression (8), we need the occupation factors of single-particle states. We can determine the occupation factors by constructing the overlap matrix of time-dependent single-particle states in the right side of the separation plane [23],

$$\langle i|j\rangle_R = \int d^3r\, \phi^*_i(\mathbf{r},t)\,\phi_j(\mathbf{r},t)\,\theta(x - x_0), \tag{9}$$

where the separation plane is at $x = x_0$. In this expression, $\phi_i(\mathbf{r},t)$ denote single-particle states originating from either the target or the projectile. The overlap matrix in the left side $\langle i|j\rangle_L$ is defined similarly. Occupation factors n_α associated with the left and right sides on the separation plane are obtained by diagonalizing the corresponding overlap matrix. At large relative distance, the occupation factors can be grouped into two classes. We first consider the left subsystem that initially contains the projectile. States with eigenvalues of $\langle i|j\rangle_L$ close to one will correspond to single-particle states originating from the projectile side (left side), while those with eigenvalues close to 0 correspond to single-particle states originating from the target (right side) and that are penetrated to the left. Because in the entrance channel changes of occupation factors are small, instead of carrying out diagonalization, we can use first-order perturbation theory to determine occupation factors. In first-order perturbation theory, eigenvalues of the overlap matrices $\langle i|j\rangle_L$ are given by $n_\alpha \approx \langle i|i\rangle_L \equiv n_i$, where $|i\rangle$ denotes a complete basis of the projectile including initially unoccupied states. As an example, Fig. 9 shows the evolution of occupation factors n_i for six neutron single-particle states initially corresponding to $1s_{1/2}$, $p_{3/2,\pm3/2}$, $p_{1/2}$, $d_{5/2,\pm5/2}$, $2s_{1/2}$, and $d_{3/2,\pm3/2}$ states (with the notation ℓ_{j,j_z}) as a function of R for the ^{40}Ca + ^{40}Ca reaction at $E_{\rm c.m.} = 100$ MeV. Occupation factors decrease monotonically as R decreases but remains still close to one around the Coulomb barrier $R_B \approx 9.8$ fm.

To have a simple estimate of the excitation energy, we further assume that occupation factors $n_i = \langle i|i\rangle_L$ have the same shape as the Fermi-Dirac distribution. Then, only the tail of the distribution contributes to the excitation energy; consequently, the excitation energy of the left subsystem can approximately be calculated according to

$$E^*_L(t) \approx 2\sum_{i=1}^{A_P} \left(\varepsilon^0_i - \varepsilon^\tau_F\right)\left(\langle i|i\rangle_L - n^0_i\right), \tag{10}$$

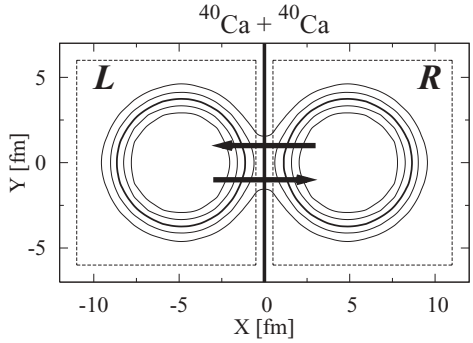

FIG. 8. Schematic illustration of the ^{40}Ca + ^{40}Ca reaction in the entrance channel at relative distance $R = 9.8$ fm. The different curves correspond to iso-contours of total nuclear density while the vertical line denotes the separation plane.

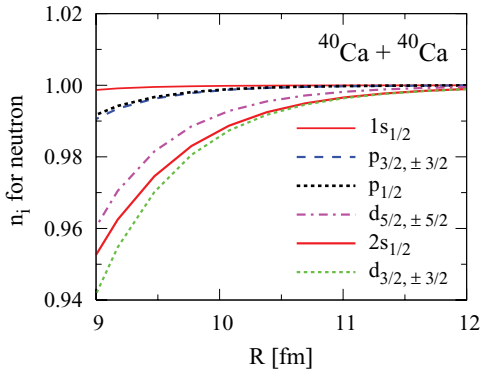

FIG. 9. (Color online) Occupation factors $n_i = \langle i|i\rangle_L$ for neutron single-particle states as a function of R for the ^{40}Ca + ^{40}Ca reaction at $E_{\rm c.m.} = 100$ MeV.

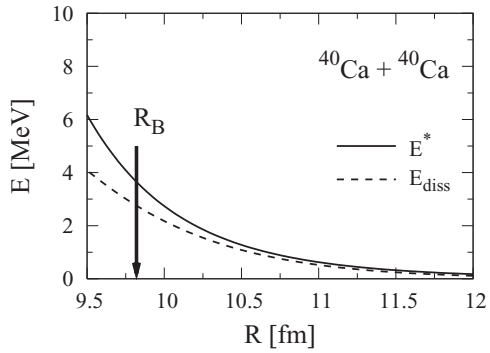

FIG. 10. Comparison of internal excitation energy E^* (solid line) with dissipated energy $E_{\rm diss}$ from Eq. (6) (dashed line) as a function of R for the ^{40}Ca + ^{40}Ca reaction at $E_{\rm c.m.} = 100$ MeV. The vertical arrow indicates the position of the Coulomb barrier radius.

where summation runs over the states that are initially occupied in the projectile. Similar expression can be found for the excitation E^*_R of the right subsystem. In Fig. 10, the total excitation energy $E^* = E^*_R + E^*_L$ (solid line) is compared with the dissipated energy $E_{\rm diss}$ given by Eq. (6) (dashed line) for the ^{40}Ca + ^{40}Ca reaction at $E_{\rm c.m.} = 100$ MeV. The agreement between the two quantities is quite good all the way up to the barrier distance $R > R_B$. Near equality of the excitation energy and the dissipated energy provides a consistency check for the friction coefficient extracted from the TDHF simulations.

V. SUMMARY

Using a macroscopic reduction procedure of the mean-field theory proposed in Refs. [6,15,16], we extract the friction coefficient associated with one-body energy dissipation in the entrance channel of heavy-ion fusion reactions. The magnitude and form factor of the reduced friction coefficient have a universal property for various reactions that are investigated. Nucleus-nucleus potentials obtained with the same method exhibit energy dependence. In a similar manner, magnitude and form factor of the extracted friction coefficient depend on the beam energy as well. It is observed that the rate of dissipation increases as the beam energy approaches the Coulomb barrier. The enhancement of the dissipation rate at low energy is a consequence of early neck formation and increasing rate of particle exchange between projectile-like and target-like nuclei. The order of magnitude of dissipation deduced from TDHF is in agreement with microscopic calculations of the friction coefficient based on the linear response theory. We estimate the excitation energy in the entrance channel by other methods. Very close agreement found between the calculated excitation energy and the dissipated energy determined from the friction coefficient provides further support for the validity of the extracting procedure for dissipation that we employed.

We should note that the mean-field dynamics provide a good approximation for describing nuclear collisions at bombarding energies per nucleon smaller than the average nucleon binding energy. Consequently, at low energies, nuclear dissipation is dominated by the one-body dissipation mechanism (nucleon exchange plus excitation of surface modes) based on the mean-field dynamics. This is clearly illustrated by the fact that friction coefficients extracted with the DD-TDHF method are compatible with those used in other models in which dissipative effects have been adjusted to describe experiments. At higher bombarding energies, two-body dissipation mechanism due to nucleon-nucleon collisions, which is neglected in the mean-field dynamics, becomes more important. However, thus far, we are not aware of any experimental signature in nuclear fusion studies that clearly identifies the fraction of dissipation mechanism due to the mean-field dynamics and the fraction due to the two-body dissipation mechanism in the entrance channel of heavy-ion reactions.

ACKNOWLEDGMENTS

We thank P. Bonche for providing us with the three-dimensional TDHF code. We also are grateful to B. Avez, D. Boilley, and C. Simenel for discussions. One of us (S.A.) gratefully acknowledges CNRS for financial support and GANIL for warm hospitality extended to him during his visit. This work is supported in part by US DOE Grant DE-FG05-89ER40530.

[1] W. U. Schröder and J. R. Huizenga, in *Treatise on Heavy-Ion Science,* edited by D. A. Bromley (Plenum, New York, 1984), Vol. 2, p. 115.
[2] D. H. E. Gross and H. Kalinowski, Phys. Lett. **B48**, 302 (1974); Phys. Rep. **45**, 175 (1978).
[3] J. Blocki, Y. Boneh, J. R. Nix, J. Randrup, M. Robel, A. J. Sierk, and W. J. Swiatecki, Ann. Phys. (NY) **113**, 330 (1978).
[4] J. Randrup and W. J. Swiatecki, Ann. Phys. (NY) **125**, 193 (1980); Nucl. Phys. **A429**, 105 (1984).
[5] D. Hilscher and H. Rossner, Ann. Phys. Fr. **17**, 471 (1992); in *Proceedings of the International School-Seminar on Heavy Ion Physics, Dubna, Russia, 1993*, Vol. I, p. 230.
[6] S. E. Koonin, Prog. Part. Nucl. Phys. **4**, 283 (1980).
[7] J. W. Negele, Rev. Mod. Phys. **54**, 913 (1982).
[8] A. S. Umar, M. R. Strayer, and P.-G. Reinhard, Phys. Rev. Lett. **56**, 2793 (1986).
[9] P.-G. Reinhard, A. S. Umar, K. T. R. Davies, M. R. Strayer, and S.-J. Lee, Phys. Rev. C **37**, 1026 (1988).
[10] J. A. Maruhn, P.-G. Reinhard, P. D. Stevenson, and M. R. Strayer, Phys. Rev. C **74**, 027601 (2006).
[11] K.-H. Kim, T. Otsuka, and P. Bonche, J. Phys. G **23**, 1267 (1997).
[12] T. Nakatsukasa and K. Yabana, Phys. Rev. C **71**, 024301 (2005).
[13] A. S. Umar and V. E. Oberacker, Phys. Rev. C **73**, 054607 (2006).
[14] D. M. Brink and F. Stancu, Phys. Rev. C **24**, 144 (1981).
[15] D. Lacroix, arXiv:nucl-th/0202063.
[16] K. Washiyama and D. Lacroix, Phys. Rev. C **78**, 024610 (2008).
[17] A. S. Umar and V. E. Oberacker, Phys. Rev. C **74**, 021601(R) (2006).

[18] C. Simenel and B. Avez, Int. J. Mod. Phys. E **17**, 31 (2008).
[19] P. Bonche, H. Flocard, P. H. Heenen, S. J. Krieger, and M. S. Weiss, Nucl. Phys. **A443**, 39 (1985).
[20] P. Bonche, H. Flocard, and P. H. Heenen, Comput. Phys. Commun. **171**, 49 (2005).
[21] G. G. Adamian, R. V. Jolos, A. K. Nasirov, and A. I. Muminov, Phys. Rev. C **56**, 373 (1997).
[22] H. Hofmann and P. J. Siemens, Nucl. Phys. **A257**, 165 (1976).
[23] C. H. Dasso, T. Døssing, and H. C. Pauli, Z. Phys. A **289**, 395 (1979).